

Numerical simulations of disc-planet interactions

Richard P. Nelson · Sijme-Jan Paardekooper

Received: date / Accepted: date

Abstract The gravitational interaction between a protoplanetary disc and planetary sized bodies that form within it leads to the exchange of angular momentum, resulting in migration of the planets and possible gap formation in the disc for more massive planets. In this article, we review the basic theory of disc-planet interactions, and discuss the results of recent numerical simulations of planets embedded in protoplanetary discs. We consider the migration of low mass planets and recent developments in our understanding of so-called type I migration when a fuller treatment of the disc thermodynamics is included. We discuss the runaway migration of intermediate mass planets (so-called type III migration), and the migration of giant planets (type II migration) and the associated gap formation in this disc. The availability of high performance computing facilities has enabled global simulations of magnetised, turbulent discs to be computed, and we discuss recent results for both low and high mass planets embedded in such discs.

Keywords planet formation · accretion discs · numerical simulations

1 Introduction

Planets are believed to form in the circumstellar discs of gas and dust that are observed around young stars (1). Within these discs, sub-micron sized interstellar dust grains collide and stick, slowly growing to form bodies comparable in mass to the Earth (M_{\oplus}) via a multi-stage process which

involves bodies of increasing size colliding and sticking. These planetary bodies which form with masses up to $\simeq 10 M_{\oplus}$ can accrete gas envelopes, leading to the formation of a gas giant planet (2), a process which, models predict, requires a few million years. The precursor $\simeq 10 M_{\oplus}$ bodies which accrete gas are usual referred to as planetary cores, and their formation is most efficient at locations in the disc where the density of solids is highest. Thus gas giant planets are thought to form in the cool disc regions beyond the ‘snowline’, where volatiles can condense into ice grains. In most disc models, and apparently in our own early Solar System, the snowline is located at a radius ~ 3 AU from the central star. The discovery of the first extrasolar planet in 1995 (3), a gas giant planet orbiting at 0.05 Astronomical Units (AU) from the star 51 Pegasi therefore came as a big surprise, and posed a problem for planet formation theory.

The solution to this problem is thought to be that planets such as 51 Peg b probably did form several AU away from the star, but migrated inward afterwards, while still embedded in the circumstellar disc. The large number of extrasolar planets now known (more than 350 at the time of writing), with broad variation in their masses and orbital configurations, indicates that migration is a common phenomenon during planet formation.

Prior to the discovery of extrasolar planets, it was already known that embedded bodies experience a force from the surrounding gas disc (4; 5; 6; 7) leading to orbital migration. This can be appreciated in a qualitative way from Fig. 1, where we show the surface density perturbation in a disc by a low-mass planet. The planet launches two tidal waves that are sheared into spiral waves by differential rotation in the disc. The gravitational pull from these waves leads to orbital migration of the planet.

Disc-planet interaction has become the focus of intense research since 1995, and three types of migration can be distinguished: Type I migration for low-mass planets (compara-

R.P. Nelson
Astronomy Unit, Queen Mary University of London, Mile End Rd,
London, E1 4NS, U.K.
E-mail: R.P.Nelson@qmul.ac.uk

S.-J. Paardekooper
DAMTP, Wilberforce Road, Cambridge CB3 0WA, U.K.
E-mail: S.Paardekooper@damtp.cam.ac.uk

ble to the Earth), which do not strongly perturb the surrounding disc, Type II migration for high-mass planets (comparable to Jupiter), which open deep gaps around their orbit, and Type III migration for intermediate-mass planets (comparable to Saturn), embedded in massive discs (8).

A significant fraction of the research in this area has utilised numerical simulations, and a number of insights have been gained from the results of such simulations which have subsequently been interpreted within the framework of an analytic model. The increasing availability of parallel computing facilities, combined with the development of simulation codes, has allowed increasingly complex simulations to be performed, including physics such as MHD turbulence and radiation transport. In this article we will review the basic theory of disc-planet interactions, highlight some recent developments, and summarise the state of the field as it currently stands.

2 Type I migration

Type I migration is thought to apply to low-mass planets (approximately $1\text{--}20 M_{\oplus}$). It is important to understand this regime, because not only does it apply to terrestrial planets, also the solid cores of gas giant planets have been subject to Type I migration before they obtained their gaseous envelope. This stage in giant planet formation requires more than 10^6 years (2). In this section, we will review the basic theory of Type I migration, focusing on laminar (non-turbulent) discs.

Type I migration has long been regarded as the simplest migration mechanism to understand. Since low-mass planets induce only small perturbations in the disc, a linear analysis should provide accurate estimates of the migration rate (9). These can later be verified by numerical hydrodynamical simulations (e.g. 10).

2.1 Linear analysis

It is convenient to express the perturbing potential due to the planet acting on the disc Φ_p as a Fourier series

$$\Phi_p(r, \varphi, t) = -\frac{GM_p}{|\mathbf{r} - \mathbf{r}_p|} = \sum_{m=0}^{\infty} \Phi_m(r) \cos(m\varphi - m\Omega_p t), \quad (1)$$

where φ is the azimuthal angle and Ω_p is the orbital frequency of the planet, and to evaluate the response of the disc due to each component separately. For simplicity, we will consider only two-dimensional, isothermal discs in this section. The vertically integrated pressure is then given by $P = c^2 \Sigma$, where c is the sound speed and Σ is the surface density of the disc defined by $\Sigma = \int_{-\infty}^{\infty} \rho dz$. In vertical hydrostatic equilibrium, the pressure scale height of the disc equals $H = c/\Omega$, where Ω is the angular velocity of the

disc. A typical disc has $h \equiv H/r \approx 0.05$. The unperturbed surface density follows a power law in radius, $\Sigma \propto r^{-\alpha}$.

When working with discs, angular momentum is a key quantity, dominating the dynamics. The angular momentum of the planet is $J_p = M_p r_p^2 \Omega_p \propto \sqrt{r_p}$ for a circular orbit. Therefore, changes in angular momentum are directly related to a change in orbital radius, which makes the torque, the change in angular momentum, an important quantity to measure.

Writing the perturbed surface density as

$$\Sigma'(r, \phi, t) = \Sigma'_m(r) \exp(im\phi - im\Omega_p t), \quad (2)$$

one can numerically solve the linearised fluid equations to obtain the disc response. The torque on the planet,

$$\Gamma = \int_{\text{Disc}} \Sigma \mathbf{r} \times \nabla \Phi_p dS, \quad (3)$$

is directly related to the imaginary part of the surface density perturbation:

$$\frac{d\Gamma_m}{dr} = -\pi m \Phi_m \mathcal{I} m(\Sigma'_m), \quad (4)$$

and the torque Γ_m can be found by integrating over the whole disc. The total torque is equal to the sum over all Γ_m .

Neglecting pressure effects, the disc can exchange angular momentum with the planet at a Lindblad resonance, which is located at a position in the disc where $m(\Omega - \Omega_p) = \pm \kappa$, or at a corotation resonance, where $\Omega = \Omega_p$. Here, κ is the epicyclic frequency, equal to Ω in a Keplerian disc. At a Lindblad resonance, a pressure wave is excited that propagates away from the planet, which cause an oscillatory disc response in the solutions to linearised equations described above. The waves transport angular momentum, resulting in a torque on the planet. The outer wave removes angular momentum from the planet, while the inner wave gives angular momentum to the planet. The torque therefore depends on the difference in the strengths of the two waves.

There are several effects that conspire to make the outer wave stronger (11), the most important one being that outer Lindblad resonances are located closer to the planet than inner Lindblad resonances. Therefore, for all reasonable surface density profiles the total Lindblad torque on the planet is negative, resulting in inward migration. The most recent linear calculations for a 2D disc (9) resulted in a Lindblad torque

$$\Gamma_{L,\text{lin}} = -(3.2 + 1.468\alpha) \frac{q^2}{h^2} \Sigma_p r_p^4 \Omega_p^2, \quad (5)$$

where q denotes the mass of the planet in units of the central mass, r_p denotes the orbital radius of the planet and Σ_p is the surface density at the location of the planet. Note that α is usually thought to be positive, resulting in a negative torque on the planet.

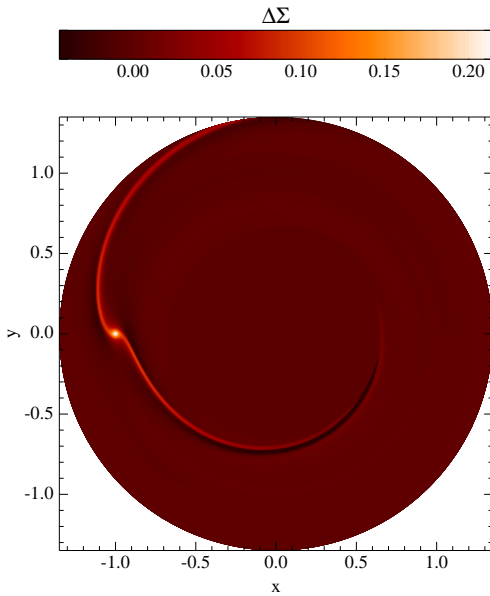


Fig. 1 Surface density perturbation for a $4 M_{\oplus}$ planet (located at $(x, y) = (-1, 0)$) embedded in a disc with $h = 0.05$, showing the prominent spiral wakes associated with Lindblad torques.

In figure 1 we show the surface density perturbation due to a low-mass planet from a numerical hydrodynamical calculation. Clearly visible are the two spiral waves launched by the planet that result in the above Lindblad torque.

As mentioned above, angular momentum exchange also takes place at a corotation resonance. Since the location of this resonance is very close to the orbit of the planet, the resulting corotation torque is potentially very strong. Since the relative velocity of the gas and the planet is subsonic near the corotation resonance, the planet is unable to excite waves at this location (12). Semi-analytical calculations (9) result in a linear corotation torque

$$\Gamma_{c,\text{lin}} = 1.36 \left(\frac{3}{2} - \alpha \right) \frac{q^2}{h^2} \Sigma_p r_p^4 \Omega_p^2, \quad (6)$$

and therefore a total linear torque

$$\Gamma_{\text{lin}} = \Gamma_{L,\text{lin}} + \Gamma_{c,\text{lin}} = - (1.16 + 2.828\alpha) \frac{q^2}{h^2} \Sigma_p r_p^4 \Omega_p^2. \quad (7)$$

Again, since α is usually thought to be positive, we find that low-mass planets will migrate inward. In equation 6, the quantity in brackets is the power law index of the specific vorticity, or vortensity $(\nabla \times \mathbf{v})/\Sigma$, where \mathbf{v} is the velocity in the disc. The corresponding migration rate is (assuming a circular orbit):

$$\dot{r}_p = \frac{2\Gamma_{\text{lin}}}{r_p \Omega_p M_p} = - (1.16 + 2.828\alpha) \frac{q}{h^2} \frac{\Sigma_p r_p^2}{M_*} r_p \Omega_p. \quad (8)$$

A major problem with the resulting inward migration rates is that they are much too high: Type I migration would quickly take all low-mass planets, including the cores of gas giant planets, very close to or even into the central star (11).

Models of planet formation including Type I migration (13) have great difficulty explaining the observed distribution of planets.

Several mechanisms have been proposed to slow down Type I migration. Within linear theory, it is first of all important to note that the two-dimensional approximation is not valid once the gravitational sphere of influence of the planet (the Hill sphere) is smaller than the pressure scale height of the disc. It is easy to see that for a small enough planet, the upper layers of the disc do not feel the gravitational pull of the planet, while in the above two-dimensional theory they fully contribute to the torque. A torque formula that accounts for this effect reads (9)

$$\Gamma_{3\text{D},\text{lin}} = - (1.364 + 0.541\alpha) \frac{q^2}{h^2} \Sigma_p r_p^4 \Omega_p^2. \quad (9)$$

Note that the difference between the 2D and the 3D result strongly depends on the surface density profile. In favourable cases, migration speeds can be reduced by a factor of a few. In the 2D numerical simulations presented below, a gravitational softening parameter b is used to account for 3D effects in an approximate way:

$$\Phi_p = - \frac{GM_p}{\sqrt{|r - r_p|^2 + r_p^2 b^2}}. \quad (10)$$

It is expected that for $b \sim h$, 3D effects on the Lindblad torque can be captured approximately. The same may not be true for the non-linear torque discussed below. In (14), equation 9 has been successfully compared to 3D isothermal numerical simulations. Note, however, that their adopted density profile allows for weak corotation torques only.

The above analysis was simplified by neglecting magnetic fields, self-gravity and detailed thermodynamics. Including magnetic resonances in the linear analysis can reduce the torque significantly if a toroidal magnetic field is present (15). On the other hand, self-gravity tends to accelerate Type I migration due to a shift in resonances (16; 17). More recently, releasing the assumption of an isothermal disc has been the subject of intensive study, since simulations presented by (18) which included radiation transport in the disc suggest that type I migration may be stopped or reversed in a disc which cools inefficiently. A linear analysis (19) suggested that a linear effect due to the presence of a radial entropy gradient may reduce or even reverse migration. However, it was subsequently shown (20) that this effect is in fact small and can not account for the results obtained in (18).

2.2 Beyond the linear model

Although intuitively, one would expect that low-mass planets induce linear perturbations only, recent work has shown that this is not the case. In a sense, introducing a planet in

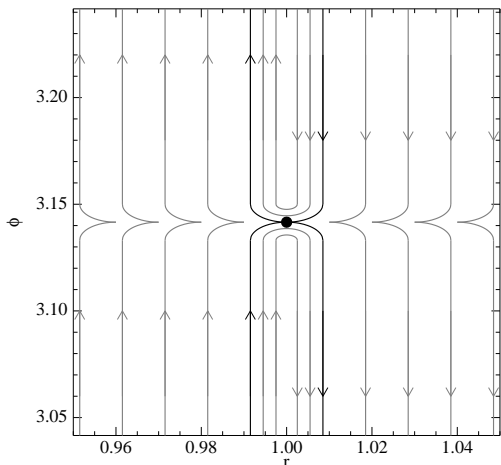


Fig. 2 Schematic view of the streamline pattern close to the planet, which is located at $(r, \varphi) = (1, \pi)$ and is denoted by the black circle. Material inside the black streamline (the separatrix) executes horseshoe turns on both sides of the planet.

a disc amounts to a singular perturbation at corotation, suggesting that the corotation torque can differ from its linear value.

The corotation torque is due to material that, on average, corotates with the planet. Two ways of obtaining the corotation torque can be found in the literature: one can perform a linear analysis of perturbed circular orbits around the corotation resonance (4; 9) (see above), or, alternatively, one can look at the expected pattern of the streamlines close to the planet (see figure 2) and analyse the torque due to material executing horseshoe turns (21). We will denote the former result the *linear corotation torque*, and the latter the *horseshoe drag*. It is important to stress that there is *no* horseshoe region in linear theory, since these bends are a genuinely non-linear phenomenon.

2.2.1 Isothermal results

Considering again two-dimensional, isothermal (or, more general, barotropic) flow, in which case specific vorticity is conserved along streamlines, it is easy to see that when executing the turn, material should change its density. Since it is forced to a different orbit by the planet, the vorticity of the material changes, and conservation of vortensity then dictates that there should be an associated change in density. This change in density is of opposite sign on the different sides of the planet, hence the planet feels a torque. This torque depends sensitively on the width of the horseshoe region x_s (21):

$$\Gamma_{c,hs} = \frac{3}{4} \left(\frac{3}{2} - \alpha \right) x_s^4 \Sigma_p r_p^4 \Omega_p^2. \quad (11)$$

Note that x_s is in units of r_p . Just as in the linear case, the horseshoe drag is proportional to the radial gradient in specific vorticity. In the special case of $\alpha = 3/2$, the density

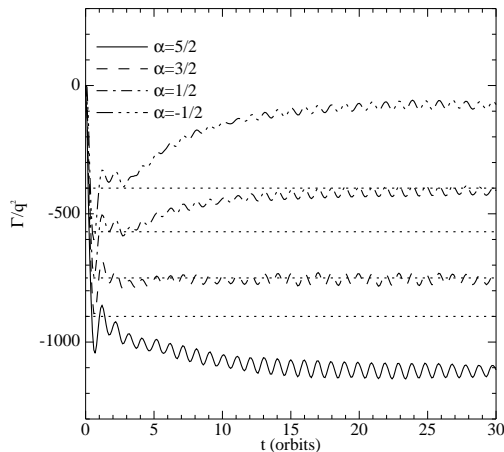


Fig. 3 Torques on a $q = 1.26 \cdot 10^{-5}$ planet ($4 M_{\oplus}$ around a Solar mass star) embedded in an inviscid disc with $h = 0.05$. All torques have been normalised to $\Sigma_p = r_p = \Omega_p = 1$. Results for different density profiles are shown, with dotted horizontal lines indicating results obtained from linear theory. A gravitational softening of $b/h = 0.6$ was used.

change needed to compensate for the change in vorticity exactly amounts to the background profile, resulting in no torque on the planet.

Until recently, it has never been clarified how equations 6 and 11 are related. There is no reason why the value of x_s , unspecified in the original theory (21), should adjust itself to match the linear torque. Detailed modeling of the horseshoe region (22) shows that $x_s \propto \sqrt{q/h}$, so that the horseshoe drag scales in exactly the same way as the linear corotation torque. The only way they differ is in magnitude, and in general the horseshoe drag is much stronger (23).

It is intuitively clear that these two distinct torques can not exist at the same time: material either follows a perturbed circular orbit or executes a horseshoe turn. At sufficiently early times after inserting the planet in the disc, therefore, before any turns can have occurred, one would expect linear theory to be valid. Once material starts to execute horseshoe turns, the linear corotation torque will get replaced by the non-linear horseshoe drag, which, as remarked above, will in general be much stronger.

This can be verified using numerical hydrodynamic simulations. Resolution is crucial, since for low-mass planets $x_s \ll h \ll 1$, and in order to obtain reliable estimates of the torque, the horseshoe bends need to be resolved. Simulation results for different values of α are displayed in figure 3, showing the total torque on the planet as a function of time. Overplotted are the results from solving the linear equations (dotted lines). It is clear that only in the case where $\alpha = 3/2$ the non-linear hydrodynamic calculations match linear theory. In this special case, the corotation torque vanishes. For all other values of α , a departure from linear theory can be seen, pointing to a stronger corotation torque than expected from linear theory. However, the total torque is consistent

with the linear corotation torque replaced by the stronger horseshoe drag, showing that indeed non-linear effects play an important role in the corotation region.

Another important aspect is the time scale to set up the torque. Since the linear corotation torque has no definite scale, it takes approximately one orbit to develop. The horseshoe drag, on the other hand, does have an intrinsic scale, namely x_s . An associated time scale is the libration time, which is basically the time it takes for a fluid element, initially at a distance x_s from the orbit of the planet, to complete one whole horseshoe orbit:

$$\tau_{\text{lib}} = \frac{8\pi}{3x_s} \Omega_p^{-1}. \quad (12)$$

It takes a fraction of the libration time for the horseshoe drag to develop, which is therefore different for different planet masses since $x_s \propto \sqrt{q}$. The transition between the linear result (obtained after approximately 1-2 orbits), and the more slowly developing non-linear horseshoe drag can be clearly seen in figure 3.

2.2.2 Extension to non-isothermal discs

These simple models of Type I migration lack a crucial ingredient: a proper treatment of the disc thermodynamics. Most previous simulations were indeed done in the locally isothermal limit, where the temperature of the disc is a prescribed and fixed function of radius. Such a model would apply if any excess energy could be radiated away very efficiently. However, in discs that can not cool efficiently (i.e. are optically thick), the presence of a radial entropy gradient leads to strong coorbital torques that can reverse the direction of migration (24). This can again be understood in terms of the horseshoe drag. When the gas is not able to cool (the adiabatic limit), entropy is conserved along streamlines. In a similar way as the vortensity gradient led to the barotropic horseshoe drag, a radial entropy gradient leads to a strong horseshoe drag related to density changes as the fluid tries to conserve its entropy when making the horseshoe turn (20). When the entropy decreases outward, this horseshoe drag gives a positive contribution to the torque.

This is illustrated in figure 4, where we compare adiabatic and isothermal simulations with $\alpha = 3/2$ for different temperature profiles (parametrised by $\beta = -d \log T / d \log r$). An adiabatic exponent $\gamma = 5/3$ was chosen. Due to the isentropic nature of linear waves, the density of the wakes is lowered by a factor γ compared to isothermal simulations, which makes the Lindblad torque a factor γ smaller. Note that the density profile is such that the barotropic corotation torque vanishes. The entropy follows a power law, initially, with index $-\xi = -\beta + (\gamma - 1)\alpha$. Therefore, the isothermal disc ($\beta = 0$) with no vortensity gradient ($\alpha = 3/2$) does have an entropy gradient ($\xi = -1$), giving rise to a strong horseshoe drag. This is clear from the grey solid line, which shows

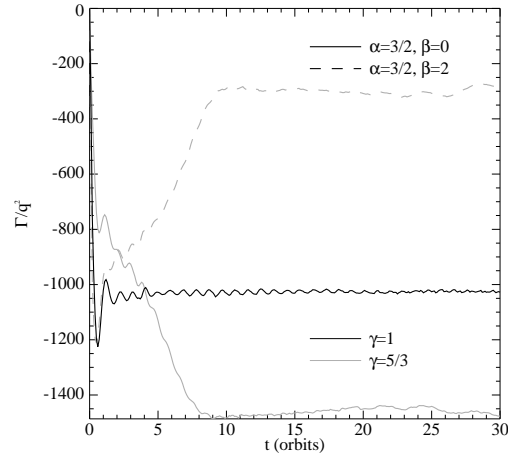


Fig. 4 Torques on a $q = 1.26 \cdot 10^{-5}$ planet ($4 M_{\oplus}$ around a Solar mass star) embedded in an inviscid disc with $h = 0.05$. All torques have been normalised to $\Sigma_p = r_p = \Omega_p = 1$. The black line indicates the isothermal result, grey curves results from adiabatic calculations for two different temperature profiles. A gravitational softening of $b/h = 0.4$ was used.

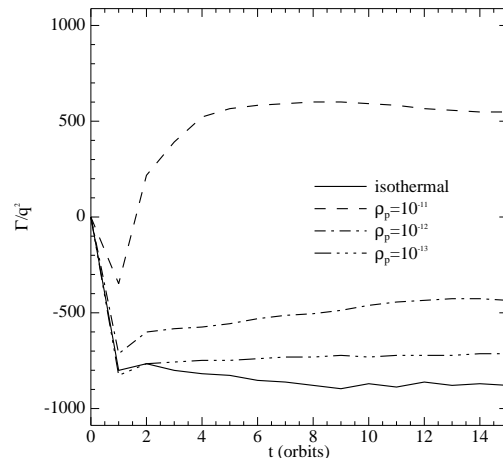


Fig. 5 Torques on a $q = 1.26 \cdot 10^{-5}$ planet ($4 M_{\oplus}$ around a Solar mass star) embedded in a 3D inviscid disc with $h = 0.05$. All torques have been normalised to $\Sigma_p = r_p = \Omega_p = 1$. Results for different midplane densities are shown, and the differences between the curves are a result of the corresponding change in opacity, which affects the cooling properties of the disc.

a large swing between 2 and 10 orbits as a result. When we modify the temperature structure to reverse the entropy gradient, a corresponding opposite swing is observed (dashed grey line in figure 4). Even without an additional contribution from a vortensity gradient, the torque is reduced by a factor of 3 compared to the linear value.

Finally, we release the two-dimensional approximation, and enable the disc to cool through radiation. The resulting 3D radiation-hydrodynamical models (18) are the most realistic simulations of low-mass planet migration so far. In figure 5, we show the results for $\alpha = 1/2$ and $\beta = 1$. Different midplane densities ρ_p were used, where $\rho_p = 10^{-11}$

g cm^{-3} approximately corresponds to the minimum mass Solar nebula at 5 AU. Note that the torques are still normalised to $\Sigma_p = 1$. Therefore, different densities mainly indicate different opacities.

The high density case is almost equivalent to an adiabatic simulation. This is easy to understand, since the disc is very optically thick in this case and basically can not cool through radiation. This again leads to a positive torque, and outward migration. Lowering the density leads to more efficient cooling, and one would expect to return to the isothermal result when the opacity is low enough. This is indeed the case: upon decreasing the density by a factor of 10 the torque is already negative, and with another factor of 10 we can almost reproduce the isothermal result. Therefore, the entropy-related horseshoe drag is important in the dense inner regions of protoplanetary discs. This mechanism can then act as a safety net for low-mass planets, since they stop their inward journey as soon as they reach the dense inner regions of the disc.

2.2.3 Saturation

In absence of any diffusive process in the disc, the horseshoe region is a closed system, and it can therefore only give a finite amount of angular momentum to the planet. Phase mixing leads to a flattening of the vortensity/entropy profiles, which results in a vanishing torque after the gas has made several horseshoe turns. In other words, the corotation torque saturates (25). The horseshoe region needs to be fed fresh material in order to sustain the torque. This can be done through viscous diffusion in the isothermal case (26), and it has been observed that by including a small kinematic viscosity and heat diffusion the torque can be sustained (20). This has also been shown with radiative cooling instead of heat diffusion in (27).

2.3 Outstanding issues

The non-linear torque strongly depends on the width of the horseshoe region x_s . It is therefore of critical importance to have a good physical understanding of what determines this width when three-dimensional effects are taken into account.

It is not clear yet how the entropy and vortensity related torques work together. Vortensity is not conserved in general along streamlines in 3D non-barotropic discs, but nevertheless there appears to be a contribution from the radial gradient in vortensity to the horseshoe drag in this case. A proper understanding of these processes will lead to an improved migration law for low-mass planets.

2.4 Concluding remarks

Type I planetary migration is not as well-understood as previously thought. Even in the simple isothermal case, strong deviations from linear theory occur whenever the disc has a radial gradient in specific vorticity. In other words, the corotation torque is always non-linear. Therefore, one should be careful in applying the widely used linear torque formula presented in (9). Even more so for non-isothermal discs, where a radial entropy gradient can contribute to the non-linear torque to the effect of reversing the direction of migration. In order for the torque to be sustained, some diffusion of energy and momentum is needed.

3 Type III migration

The most recently discovered migration mechanism, first referred to as runaway migration (8), relies on strong corotation torques induced by the radial movement of the planet itself as it migrates. Later, it has become known as Type III migration (e.g. 28).

3.1 Theory

We will return to the simple case of a laminar, isothermal disc. Consider the horseshoe region as depicted in the left panel of figure 6, and for now assume that it has constant specific vorticity, either through saturation or due to the initial density profile. The corotation torque therefore vanishes. If we now let the planet migrate radially, the horseshoe region as viewed in a frame comoving with the planet changes its shape (middle panel of figure 6). If the planet is moving inward, as is the case in figure 6, some fresh material from the inner disc will enter the horseshoe region, make the turn and move into the outer disc, exerting a torque on the planet in the process. It is easy to see that this torque is proportional to the migration speed, and acts to accelerate the migration. There is therefore a positive feedback loop, and the possibility of a runaway process.

The mass flow relative to a planet migrating at a rate \dot{r}_p (we assume a circular orbit, so that the semimajor axis $a = r_p$) is given by $2\pi\Sigma_s\dot{r}_p$, with Σ_s the surface density at the upstream separatrix. Since we assume the ordinary, vortensity-related corotation torque to be fully saturated, the only horseshoe drag on the planet comes from this fresh material executing a horseshoe turn, giving rise to a torque (29):

$$\Gamma_{c,3} = 2\pi\Sigma_s\dot{r}_p\Omega_p r_p^3 x_s. \quad (13)$$

The system of interest that is migrating is the planet itself, mass of gas bound within its Roche lobe, and the horseshoe region. The drift rate of this system is given by

$$(M_p + M_{\text{HS}} + M_{\text{R}})\Omega_p r_p \dot{r}_p = 4\pi r_p^2 x_s \Sigma_s \Omega_p r_p \dot{r}_p + 2\Gamma_L, \quad (14)$$

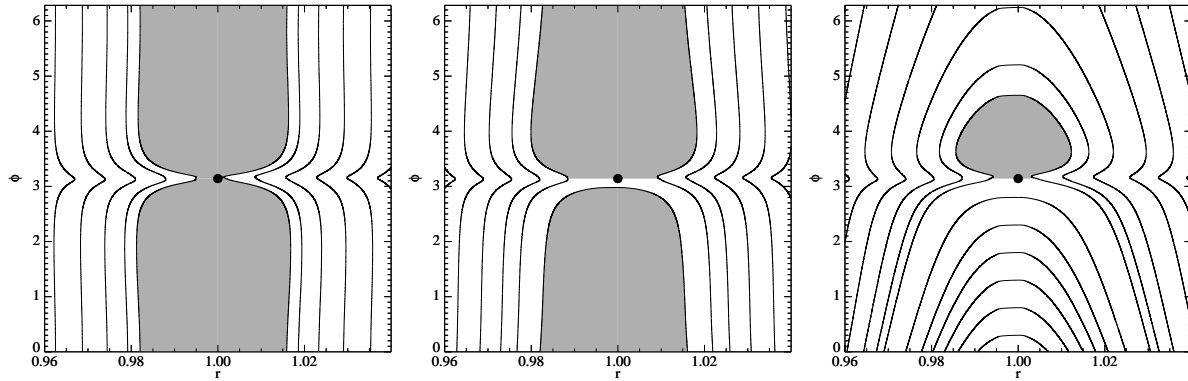


Fig. 6 Streamlines near the corotation region for different migration speeds, in a frame moving with the planet. Left panel: no migration, middle panel: slow inward migration, right panel: fast inward migration.

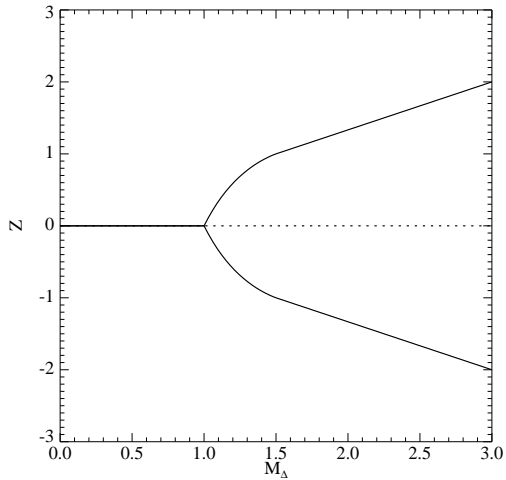


Fig. 7 Non-dimensional migration rate as a function of the mass deficit parameter M_Δ .

which can be rewritten as

$$\dot{r}_p = \frac{4\pi r_p^2 x_s \Sigma_s - M_{\text{HS}}}{M_p} \dot{r}_p + \frac{2\Gamma_L}{r_p \Omega_p}, \quad (15)$$

where we have redefined M_p as the mass of the planet plus the mass within its Roche lobe. Here, Γ_L is the Lindblad torque, which may deviate from the linear Lindblad torque due to shock formation or the appearance of a gap around the orbit of the planet. The numerator of the first term on the right hand side is called the *coorbital mass deficit* (8). Basically, this is the difference between the mass the horseshoe region would have in a disc with $\Sigma = \Sigma_s$ and its actual mass. It is clear that when this coorbital mass deficit becomes comparable to M_p , very high migration rates are possible. However, in this limit the above analysis becomes invalid. A more careful treatment (29; 30) results in:

$$Z - \frac{2}{3} M_\Delta \text{sign}(Z) (1 - (1 - |Z|)^{3/2}) = \frac{2\Gamma_L}{M_p \Omega_p r_p \dot{r}_{p,f}}, \quad (16)$$

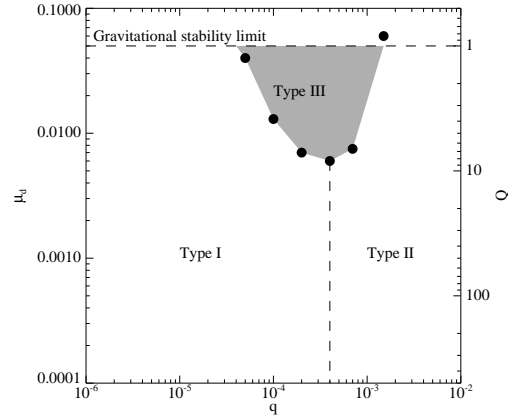


Fig. 8 The three migration regimes in disc-planet mass parameter space, for $h = 0.05$.

where M_Δ denotes the coorbital mass deficit divided by the planet mass,

$$\dot{r}_{p,f} = \frac{3x_s^2}{8\pi} r_p \Omega_p \quad (17)$$

is the drift rate required for the planet to migrate a distance x_s in one libration time, and $Z = \dot{r}_p / \dot{r}_{p,f}$. A quantity with subscript < 1 indicates that the minimum of that quantity and 1 is to be taken. Equation 16 gives rise to interesting behavior. Assuming Lindblad torques to be small, solutions to equation 16 are plotted in figure 7. For $M_\Delta < 1$, only one solution, $Z = 0$, is possible. There is a bifurcation at $M_\Delta = 1$, beyond which there are three possible solutions: steady inward or outward Type III migration, plus an unstable solution $Z = 0$. Incorporating Γ_L in this picture removes this symmetry between inward and outward migration (30), favouring migration towards the central star, although outward migration is still possible (31).

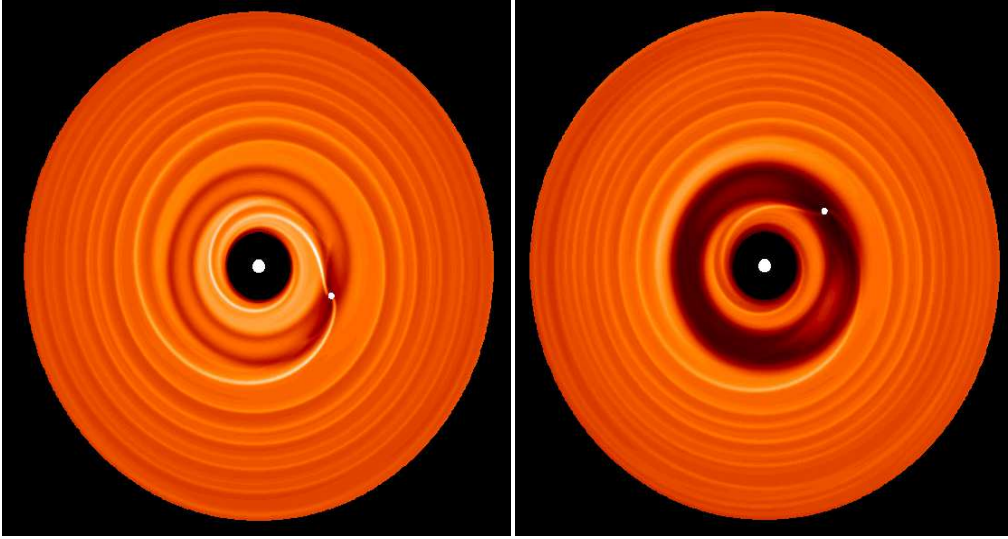


Fig. 9 This figure shows a snapshot of a planet with initial mass of 1 Jupiter mass embedded in a protoplanetary disc. Note the formation of non linear spiral waves and the accompanying gap.

3.2 Occurrence

There are different ways in which a coorbital mass deficit can be obtained. The first possibility is when the planet opens up a (partial) gap (8). Clearly, in this case there is a difference between the actual mass of the horseshoe region and the mass of the horseshoe region with $\Sigma = \Sigma_s$, hence there is a coorbital mass deficit. For a high enough disc mass, this deficit can become comparable to the planet mass. More massive planets require a more massive disc to enter the Type III migration regime. On the other hand, low-mass planets do not open up a gap and therefore their coorbital mass deficit is zero. It turns out that in a typical disc, Saturn-mass planets are most susceptible to Type III migration (8). This is depicted in figure 8, where we show the regime of Type III migration for different disc masses. Here, $\mu_d = \pi r_p^2 \Sigma_p / M_*$ is a dimensionless disc mass parameter, and Q is the corresponding Toomre stability parameter against fragmentation. For the Minimum Mass Solar Nebula (MMSN) and $h = 0.05$, $Q > 10$ inside 10 AU, making Type III migration unlikely. However, the MMSN is effectively a lower limit on the true disc mass profile, and for massive discs Type III migration may be an important effect.

Another way for a coorbital mass deficit to arise is when the background disc has a sharp edge. This was studied for Jupiter-mass planets ($q = 0.001$) in (28; 31). Such a coorbital mass deficit would also affect low-mass planets, but this has not been studied so far.

Type III migration is a numerically challenging problem, since it strongly depends on material close to the planet. For example, in the above analysis we redefined the planet mass to include all material inside the Roche lobe. If the planet obtains a significant envelope, torques from within the Roche

lobe can be large (32) and oppose Type III migration. However, since self-gravity is neglected, this material has effectively no inertia, making this calculation inconsistent (29).

To make further progress and deal with such a massive envelope, it is necessary to incorporate effects of self-gravity, at least in an approximate way (33). Moreover, to avoid an artificially large mass build-up inside the Roche lobe due to the isothermal approximation, a temperature profile for the envelope needs to be supplied. Only then can simulations of Type III migration, including torques from inside the Roche lobe, be shown to be converged (33).

Type III migration can be very fast. The typical time scale is $r_p / \dot{r}_{p,f} = 2/3x_s^2$ orbits. For $x_s = h$, appropriate for Saturn-mass planets (22), the migration timescale is approximately 200 orbits, or 2360 year for a planet starting at 5.2 AU. However, it is not clear at this point how long the coorbital mass deficit can be retained. For example, unless the surface density profile decreases steeply with radius, the coorbital mass deficit will naturally decrease as the planet moves inward because of the changing factor $r_p^2 \Sigma_s$ in equation 15. Outward Type III migration does not suffer from this effect, but simulations show that in this case the planet acquires a very massive envelope that pulls it into the Type II regime (31). Therefore, it seems that Type III migration is of limited importance for high-mass planets, changing the semimajor axis by a factor of a few (28; 31).

4 Type II migration in viscous, laminar discs

When a planet grows in mass, the spiral density waves excited by the planet in the disc can no longer be treated as linear perturbations in the manner described in section 2. The planetary wake becomes a shock-wave in the vicinity

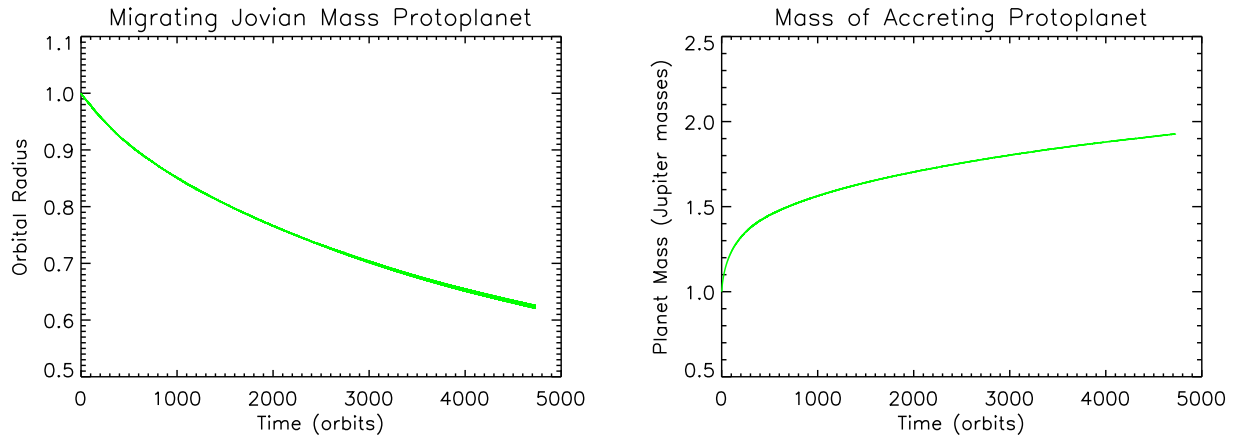


Fig. 10 The left panel shows the orbital radius of giant planet as it migrates in the disc model described in the text. The right panel shows the mass of the planet as it concurrently accretes gas from the disc.

of the Lindblad resonances where it is launched. Shock dissipation, as well as the action of viscosity, leads to the deposition of angular momentum associated with the spiral wave locally in the disc. Material is thus pushed away from the location of the planet on either side of its orbital location, and an annular gap begins to form, centred on the planet semimajor axis. The equilibrium structure and width of the gap is determined by a balance between the gap-closing viscous and pressure forces and gap-opening gravitational torques (e.g. 34).

In order for a gap to form and be maintained, two basic conditions must be satisfied. The first is that the disc response, *via* the launching of spiral wakes, should be non linear, such that gravitational forces due to the planet overwhelm pressure forces in the neighbourhood of the planet. This condition for non linearity is equivalent to the planet Hill sphere radius exceeding the disc vertical scale height, and may be expressed mathematically as:

$$a \left(\frac{M_p}{3M_*} \right)^{1/3} > H. \quad (18)$$

where a is the planet semimajor axis. The second condition is that angular momentum transport by viscous stresses in the disc be smaller than planetary tidal forces. This can be expressed approximately as

$$\frac{M_p}{M_*} > \frac{40a^2\Omega}{v}. \quad (19)$$

where v is the kinematic viscosity. For more discussion about these aspects of gap opening, see the following papers (35; 36; 37; 34).

For standard disc parameters, $H/r = 0.05$, and $v/(a^2\Omega) = 10^{-5}$, equation (18) gives $M_p/M_* > 3.75 \times 10^{-4}$, while equation (19) gives $M_p/M_* > 4 \times 10^{-4}$. The estimates are in reasonable agreement with the results of numerical simulations of gap opening by (36) and (38). Accordingly, for typical protoplanetary disk parameters, we can expect that a planet

with a mass exceeding that of Saturn will begin to open a noticeable gap.

Because the disc response to a massive embedded protoplanet is non linear, the study of the orbital evolution and gas accretion by such a planet has been the subject of extensive study *via* numerical simulations. Both 2D (e.g 36; 38; 37; 39) and 3D simulations (40; 41) have been performed, and overall the results found in these studies are in good agreement. Differences obviously arise in the details of the gas flow near the planet when comparing 2D and 3D simulations, but the global properties of the models are otherwise similar as the gas is pushed away from the planet vicinity by the process of gap opening.

Two snapshots from a 2D simulation of a disc with $H/r = 0.05$ and $v/(a^2\Omega) = 10^{-5}$ are shown in figure 9, where the initial mass of the planet $M_p = 1 M_{\text{Jup}}$ (where M_{Jup} is Jupiter's mass). The formation of a deep annular gap in the vicinity of the planet is apparent. The parameters used in this simulation are such that both the condition for non linearity and the condition for tides to overwhelm viscous stresses are satisfied, as described above.

The evolution of the planet semimajor axis is shown in the left panel of figure 10. As the gap forms and the planet migrates inward, the migration rate drops significantly below that which is predicted for type I migration. Once a clean gap is formed, the planet orbital evolution is controlled by the rate at which the outer gap edge viscously evolves, such that the migration time, τ_{mig} , can be approximated by

$$\tau_{\text{mig}} \simeq \frac{2r_p^2}{3v}. \quad (20)$$

For typical disc parameters the time to migrate from a distance of $r_p = 5$ AU to the central star is $\tau_{\text{mig}} \simeq 2 \times 10^5$ years.

As the planet mass increases, or the disc mass decreases, the inertia of the planet can become important and begin to slow the migration. This occurs when the local disc mass

contained within the orbital radius of the planet falls beneath the planet mass ($\pi r_p^2 \Sigma(r_p) < M_p$). In this case the migration rate is controlled by the rate at which mass can build-up at the edge of the gap such that the disc mass becomes comparable to the planet mass locally (42). The slowing of migration is apparent in the left panel of figure 10, and a simple linear extrapolation of the migration history indicates that the time required for this planet to migrate into the central star is $\simeq 3 \times 10^4$ orbits (or $\sim 3 \times 10^5$ years for a planet initially located at 5 AU). The right hand panel of figure 10 shows the evolution of the planet mass as it accretes gas from the disc. The mass accretion rate is slowed by the formation of the gap, but nonetheless gas is still able to diffuse through the gap onto the planet allowing it to grow. Linear extrapolation of the planet mass shown in figure 10 indicates that the planet will have grown to a mass of $M_p \simeq 3.5 M_{\text{Jup}}$ by the time it reaches the central star, such that migration and concurrent gas accretion occur during the gap opening phase of giant planet formation.

The simulations for gap forming planets presented in this section indicate that planets grow substantially through continued gas accretion as they migrate. This raises an interesting question about the type of correlation which expected between planetary semimajor axes and masses. Taken at face value, a model which predicts that planets grow as they migrate inward will predict an inverse correlation between planetary mass and semimajor axes. The strength of this correlation will be weakened by variations in protoplanetary disc masses, planet formation times, disc lifetimes etc, but if these parameters are peaked around certain typical values in nature, then the correlation should be apparent in the extrasolar planet data. The absence of such a correlation may in part be explained by post-formation interaction within a planetary system, leading to significant gravitational scattering. The possibility that significant migration may occur prior to the last stages of giant planet formation may also be important. Nonetheless, indirect evidence for the past occurrence of Type II migration in some extrasolar planetary systems *is* provided by multi-planet systems which display the 2:1 mean motion resonance (or other resonances of low degree). Such a configuration is most naturally explained by two giant planets undergoing convergent migration at rates predicted by Type II migration theory, as illustrated by the numerical simulations presented in (e.g. 43; 44).

4.1 Outstanding issues

It has turned out to be difficult to improve on the non-self-gravitating, isothermal results in which gas inside the Roche lobe is considered to be part of the planet (8). Approximate corrections for self-gravity and non-isothermality are necessary to make progress on high-mass planets (33). The first fully self-gravitating calculations indicate that this can have

important effects (45). More work is necessary in this area, also to completely release the isothermal assumption to obtain a realistic envelope structure for the planet.

5 Turbulent protoplanetary discs

The majority of calculations examining the interaction between protoplanets and protoplanetary discs have assumed that the disc is laminar. The mass accretion rates inferred from observations of young stars, however, require an anomalous source of viscosity to operate in these discs. The most likely source of angular momentum transport is magnetohydrodynamic turbulence generated by the magnetorotational instability (MRI) (46). Numerical simulations have been performed using the local shearing box approximation (see reference 47, for a review) and using global geometry (e.g. 48). In each of these set-ups, runs have been conducted using non stratified models in which the vertical component of gravity is ignored, and in more recent work the vertical component of gravity has been included in shearing box (49) and global models (50, and references therein). These model indicate that the nonlinear outcome of the MRI is vigorous turbulence, and dynamo action. Recent work has indicated that the picture is more complicated than previously thought, with there being a strong dependence of the saturated state of the turbulence on the value of the magnetic Prandtl number (51; 52).

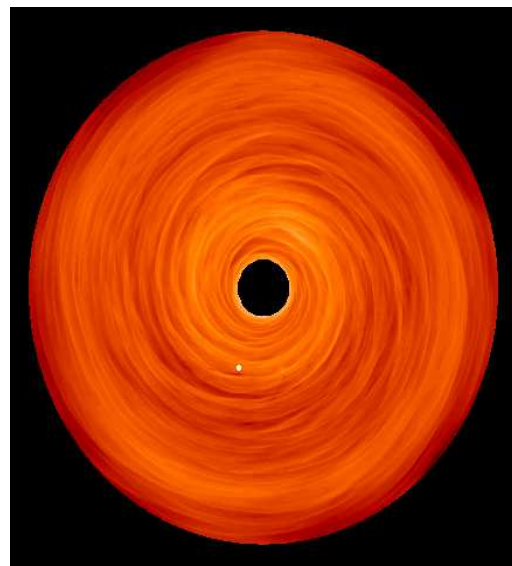


Fig. 11 This figure shows a snapshot of a $10 M_{\oplus}$ protoplanets embedded in the turbulent protoplanetary disc model described in the text.

Prior to the realisation that the strength of the MHD turbulence depends on the Prandtl number, it was recognised that non ideal MHD effects might be important in protoplanetary discs. The ionisation fraction in cool, dense pro-

toplanetary discs is expected to be small in the planet forming region between 0.5 – 10 AU. Only the surface layers of the disc, which are exposed to external sources of ionisation such as X-rays from the central star or cosmic rays, are likely to be sufficiently ionised to sustain MHD turbulence (e.g. 53; 54; 55; 56). Predictions about the structure and depth of the interior non turbulent “dead zone” depend on complex chemical reaction networks and the degree of dust grain depletion, issues which themselves may be influenced by the process of planet formation *via* dust grain growth.

Although there are a number of uncertainties remaining about the nature and strength of disc turbulence, it is clear that an accurate understanding of planet formation and disc-planet interaction requires the inclusion of turbulence in the models. Work conducted over the last four or five years has examined the interaction between planets of various masses and turbulent protoplanetary discs, where these studies have usually simulated explicitly MHD turbulence arising from the MRI. We now review the results of these studies, and present some more recent models.

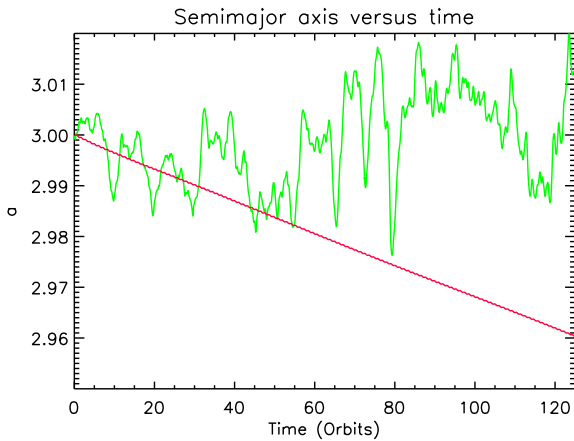


Fig. 13 This shows the variation of semimajor axis with time (measured in planet orbits at $r = 3$). The green line shows the planet evolution in a turbulent disc, the red line shows the evolution in an equivalent laminar disc.

5.1 Low mass protoplanets in turbulent discs

The interaction between low mass, non gap forming protoplanets and turbulent discs has been examined by (10; 57; 58; 59) These calculations show that interaction between embedded planets and density fluctuations generated by MHD turbulence can significantly modify type I migration, at least over time scales equal to the duration of simulations that are currently feasible ($t \sim 150$ planet orbits). The influence of the turbulence is to induce a process of ‘stochastic migration’ rather than the monotonic inward drift expected for

planets in laminar discs. The simulations presented in the papers cited above considered the interaction of planets with non stratified (no vertical component of gravity) disc models (for reasons of computational expense), but the work of (50) indicates that the amplitude of midplane density fluctuations in stratified models is weaker than in their non stratified counterparts because of magnetic buoyancy effects removing net magnetic flux from the simulation domain. It is therefore important to consider the evolution of planets in stratified models.

One such model is presented in figure 11 which shows a snapshot of the midplane density in a turbulent disc with an embedded 10 Earth mass planet. The disc model in this case has aspect ratio $H/r = 0.1$, and was initiated with a ratio of magnetic to thermal gas pressure $P_g/P_m = 25$ throughout the computational domain. As such the model is very similar to those presented in (50). The disc extends from an inner radius of 1.6 AU to 16.6 AU, and has a vertical domain covering a total of 9 scale heights. The resolution corresponds to $(N_r, N_\phi, N_\theta) = (464, 280, 1200)$. Figure 11 shows the turbulent density fluctuations are of higher amplitude than the spiral wakes generated by the planet, as the planet induced wakes are not visible against the perturbations induced by the MHD turbulence (see also 10; 58). Indeed, density fluctuations generated by turbulence in simulations are typically $\delta\Sigma/\Sigma \simeq 0.15 - 0.3$, with peak fluctuations being $\mathcal{O}(1)$. Thus, on a length scale equivalent to the disc thickness H , density fluctuations can contain more than an Earth mass in a disc model a few times more massive than a minimum mass nebula.

The left panel of figure 12 shows the variation in the torque per unit mass experienced by the planet shown in figure 11. The green line shows the torque experienced by a planet in the turbulent disc model, and the red line shows the torque experienced by the same planet in an equivalent laminar disc model (the torque value here is $\simeq 3 \times 10^{-6}$). It is clear that the planet in the turbulent disc experiences strongly varying stochastic torques whose magnitudes are significantly larger than the expected type I torques. The right hand panel shows the running time average of the torque experienced by the planet. The light blue, green and dark blue lines correspond to the torque from the outer disc, the inner disc, and the total torque, respectively. The red lines show the equivalent quantities from the laminar disc model. It is clear that while the various torque contributions are of similar magnitudes when comparing the laminar and turbulent models, the net average torque in the turbulent model is positive, indicating that the planet has migrated outward slightly over the duration of this simulation.

This expectation is confirmed by figure 13, which shows planet semimajor axes for both turbulent (green line) and laminar (red line) models. It is clear that for the duration of this run the planet in the turbulent disc has undergone

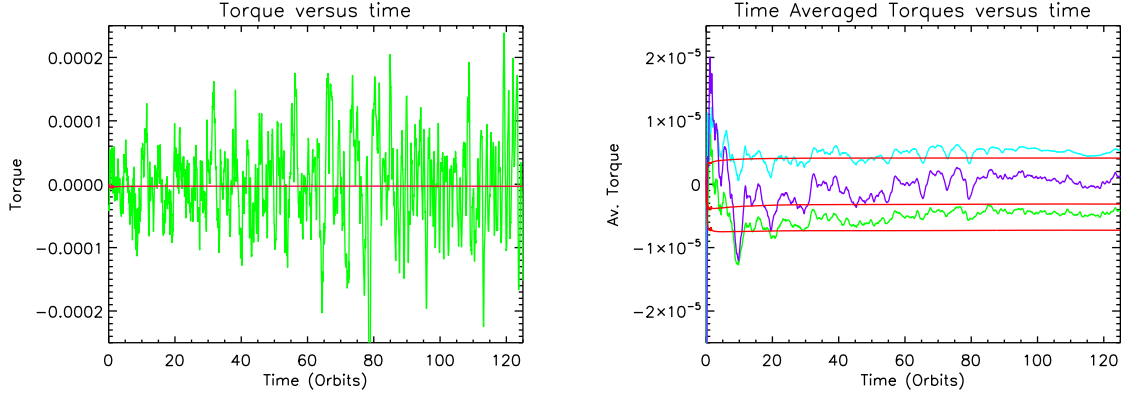


Fig. 12 The green line in left panel shows the torque experienced by the planet embedded in the turbulent disc. The red line shows the torque experienced by a planet embedded in an equivalent laminar disc. The right panel shows the time averaged values of the torques. From top to bottom, red lines are the torques from the laminar disc calculation corresponding to the disc interior to the planet, the total torque, and the disc exterior to the planet. Similarly the turquoise, purple and green lines are from the turbulent disc simulation.

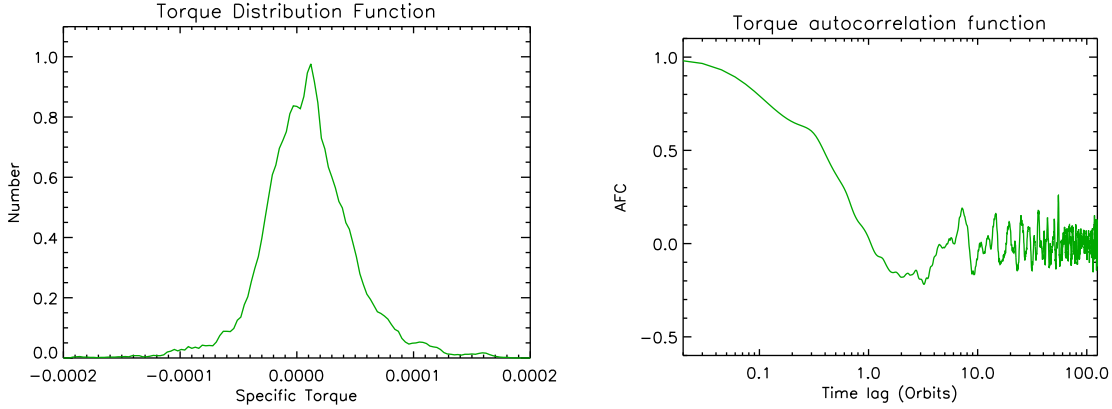


Fig. 14 The left panel shows the distribution of torques experienced by the planet embedded in the turbulent disc. The right panel shows the autocorrelation function of the torque plotted in the left panel of Fig. 13.

stochastic migration, resulting in it having moved outward slightly. A key question is whether the stochastic torques can continue to overcome type I migration over time scales up to disc life times. A definitive answer will require very long global simulations, but simple estimates can be made based on the simulated torques and their statistical properties.

If we assume that the planet experiences type I torques from the turbulent disc, on top of which are linearly superposed Gaussian distributed fluctuations with a characteristic correlation time τ_c , then we can write an expression for the time averaged torque experienced by the protoplanet, \bar{T} , in the form

$$\bar{T} = \langle T \rangle + \frac{\sigma_T}{\sqrt{t_{\text{tot}}}} \quad (21)$$

where σ_T is the standard deviation of the torque amplitude, $\langle T \rangle$ is the underlying type I torque, and t_{tot} is the total time elapsed, measured in units of the torque correlation time τ_c . In other words we treat the calculation as a simple signal-to-noise problem. Convergence toward the underlying type I value is expected to begin once the two terms on

the right hand side become equal, as the fluctuating component should begin to average out. The torque distribution function for this simulation is shown in the left panel of figure 14, and the torque autocorrelation function is shown in the right hand panel. Expressed in code units, the rms torque value is $\sim 4 \times 10^{-5}$ and the correlation time is $\tau_{\text{migr}} \simeq 1$ planet orbital period. The type I torque is $\langle T \rangle \simeq 3.5 \times 10^{-6}$, so the time over which type I torques should be apparent is 130 orbits, slightly more than the simulation run time. This prediction suggests that we should expect to see the planet begin to migrate inward in figure 13, but this clearly is not the case.

The lack of inward migration in figure 13 may just be a consequence of not having run the simulation for long enough, such that the fluctuating torques have not had time to begin to average out. The similarity between the run time of the simulation and the estimate of the time when type I effects should become apparent suggests that this may be the case. If we look at the right panel of figure 12, how-

ever, we can see that the averaged torque due to the disc that lies interior to the planet has converged to a value which is very close to that obtained in a laminar disc model. The outer disc torque, however, remains somewhat lower in amplitude, such that the net torque experienced by the planet is positive over the simulation run time. It is well known that the stochastic nature of the disc turbulence, and the associated stresses it generates, can lead to structuring of the disc radial density profile due to local variations in the effective viscous stress. This may provide a means of modifying the balance between inner and outer disc torques such that convergence to the expected type I value does not happen in practice for an individual planet in a disc, although it should happen on average for an ensemble of planets. One potential way in which the underlying type I torques may not be recovered is if local variations in the viscous stress lead to undulations in the radial density profile. In this situation the corotation torque may become important in regions where the disc surface density increases locally with radius. The effect of this is illustrated by equation (6), which shows that if the surface density profile becomes positive then the corotation torque experiences a boost because α becomes negative. This phenomenon has been dubbed a ‘planet trap’ by (60). Over longer viscous time scales such undulations in the density distribution will be smoothed out, but it is possible that planets may be able to migrate from one such density feature to another such that the next migration rate is substantially reduced.

Significantly longer simulations are required in order to examine the long term evolution of low mass planets embedded in stratified, global, turbulent disc models and to determine the efficacy of disc turbulence in modifying type I migration. Furthermore, in order to build up a statistically significant picture of the distribution of outcomes, a number of such simulations will be required. In addition, the issue of how dead zones affect the stochastic torques also needs to be examined. It is worth noting that the simulation presented in this section required approximately 55 days of wall-clock run time on 256 processing cores. Clearly a full exploration of this problem remains a very challenging computational task.

5.2 High mass protoplanets in turbulent discs

The interaction of high mass, gap forming planets with turbulent protoplanetary discs has been considered in a number of papers (61; 62; 57; 10). In all these works, the disc model considered was non stratified such that the vertical component of gravity was neglected. It is well-known, however, that the flow of material in the vicinity of a giant planet develops a well-defined three dimensional structure, such that full 3D simulations are required to examine the details of the disc-planet interaction.

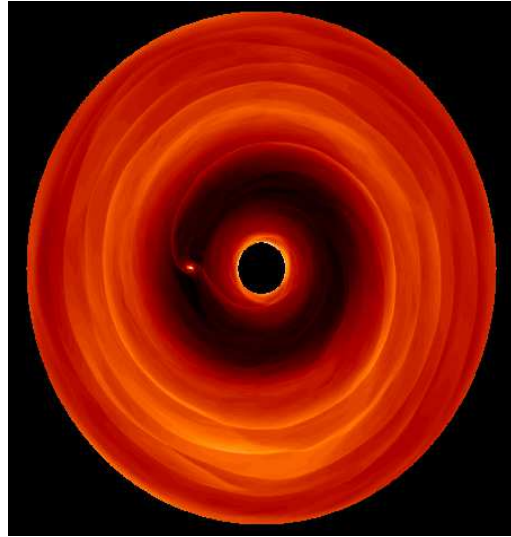


Fig. 15 This figure shows a snapshot of the disc midplane density for a protoplanet with initial mass of $1/3 M_{\text{Jup}}$ embedded in a turbulent disc. This snapshot corresponds to a time when the planet mass has reached $\simeq 4 M_{\text{Jup}}$ by accreting gas from the disc.

Figure 15 shows a snapshot of the midplane density for a turbulent disc with an embedded $4 M_{\text{Jup}}$ protoplanet. The disc model in this case is the same as that described in section 5.1 with $H/R = 0.1$. The planet had an initial mass $M_p = 1/3 M_{\text{Jup}}$ and was able to accrete gas from the disc. The gas accretion algorithm consists of the standard procedure of removing a fraction of the gas contained within one quarter of the planet Hill sphere at each time step. When magnetic fields are present in the simulation this procedure can lead to the formation of a magnetically dominant envelope forming around the planet. This problem was circumvented by allowing the gas within the planet Hill sphere to have a finite resistivity such that the field diffuses from this region as it builds up.

An initial planet mass of $M_p = 1/3 M_{\text{Jup}}$ is below the gap opening mass according to the criterion expressed by equation (18). As the planet accretes mass, however, gas is removed from the vicinity of the planet, and the growth of the planet mass allows tides to begin to open a gap once the Hill sphere radius begins to exceed the local disc scale height. This is in agreement with (57), who considered the transition from fully embedded to gap forming planets using local shearing box and global simulations of turbulent discs. These simulations showed that gap formation begins when the disc response to the planet gravity starts to become non linear. The combined Maxwell and Reynolds stresses in simulations with zero-net magnetic flux (as considered here) typically give rises to an effective viscous stress parameter $\alpha_{\text{visc}} \simeq 5 \times 10^{-3}$, such that the viscous criterion for gap formation is satisfied when the criterion for non linear disc response is satisfied. Here α_{visc} is defined to be $\alpha_{\text{visc}} = \langle T \rangle / \langle P \rangle$, where T is the total (Maxwell plus Reynolds) stress,

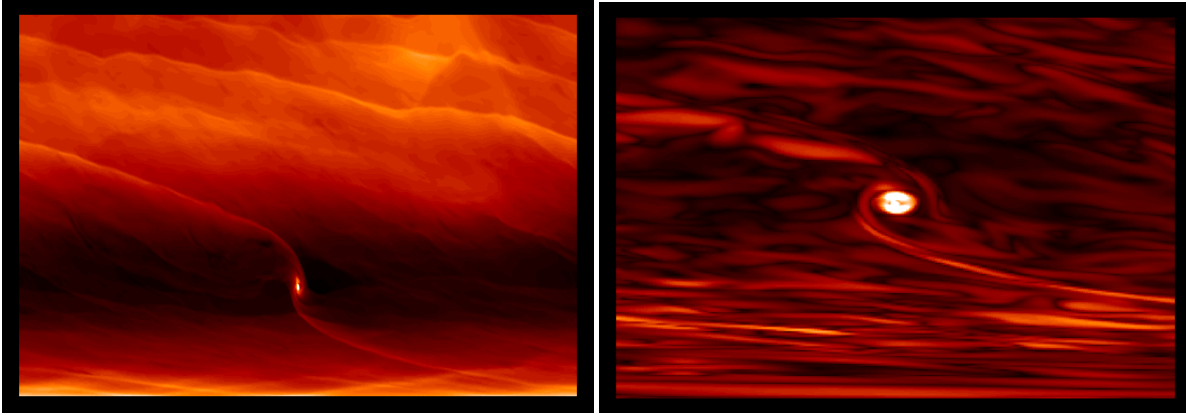


Fig. 16 The left panel shows the gas density at the disc midplane, and the right panel shows contours of the quantity B^2 at the disc midplane.

P is the thermal pressure, and angled brackets represent vertical and azimuthal averages.

Global simulations allow the net torque on the planet due to the disc to be calculated and hence the migration time to be estimated. Simulations presented in (61; 10) for massive planets indicate migration times of $\sim 10^5$ yr, in line with expectations for type II migration. The left panel of figure 16 shows the torques per unit mass experienced by the planet due to the disc as a function of time. Although gap formation has not reached a state of completion (this is found to require approximately 400 planet orbits in laminar disc runs such as those presented in section 4), such that the torques have not reached their final values, this figure can be used to estimate a lower limit on the migration time. We express this as $\tau_{\text{mig}} = j/(dj/dt)$, where j is the specific angular momentum of the planet. The specific torque at $t = 100$ orbits is $dj/dt = 2 \times 10^{-5}$, (expressed in code units). The planet specific angular momentum $j = \sqrt{3}$ such that the migration time corresponds to $\tau_{\text{mig}} = 3 \times 10^4$ years. Completion of gap formation will reduce the torques experienced by the planet considerably as the gas is pushed away from its vicinity by tides, causing the final migration time to significantly exceed this value. But, as noted in section 5.1, the run times associated with these full 3D stratified disc models only allow full 3D magnetised and stratified disc simulations to run for $\simeq 100$ orbits at the present time.

A number of interesting features arise in simulations of gap forming planets embedded in turbulent discs, which differentiate them from runs performed using laminar but viscous disc models. Comparing figure 15 with figure 9 shows that the spiral arms in the turbulent disc appear less well-defined and more diffused than in the laminar models. This point is reinforced by the left panel of figure 17, which contains a snapshot of the planet-disc system in the $r-\phi$ plane. The magnetic field topology is significantly modified in the vicinity of the protoplanet, as illustrated by the right panel in figure 17 which displays a snapshot of the quantity B^2 in the disc in the vicinity of the planet. It can be seen that the

magnetic field is compressed and ordered in the postshock region associated with the spiral wakes, increasing the magnetic stresses there. Accretion of gas into the protoplanet Hill sphere causes advection of field into the circumplanetary disc that forms there, creating a strong magnetic field in the circumplanetary disc, and this field links between the protoplanetary disc and the circumplanetary disc, producing an effect of magnetic braking of the circumplanetary material. Indeed, a direct comparison between a simulation of a $3 M_{\text{Jup}}$ protoplanet in a viscous laminar disc and an equivalent turbulent disc simulation presented by (10) suggests that mass accretion onto the planet in a magnetised disc may be enhanced by this effect. Simulations are underway at present to explore this effect within the 3D stratified model presented in this section. It is worth noting, however, that these global simulations are of modest resolution, especially when considering complex physical processes occurring within the planet Hill sphere, and more high resolution work needs to be done to examine these issues in greater detail.

6 Summary

We have reviewed recent progress in the field of disc-planet interactions in the context of orbital migration. This progress has come about to a large degree from large scale two and three dimensional simulations that have utilised the most up to date supercomputer resources. These have allowed very high resolution simulations to be performed which examine the detailed behaviour of the disc in the corotation region, leading to a fuller understanding of the potential influence of the corotation torque in modifying the migration of low mass and fully embedded planets. Simulations have also enabled the study of migration in non isothermal discs in which radiation transport is included, showing the importance of relaxing the widely used assumption that the disc gas can be treated as being locally isothermal. The inclusion of MHD effects in full 3D global simulations is now

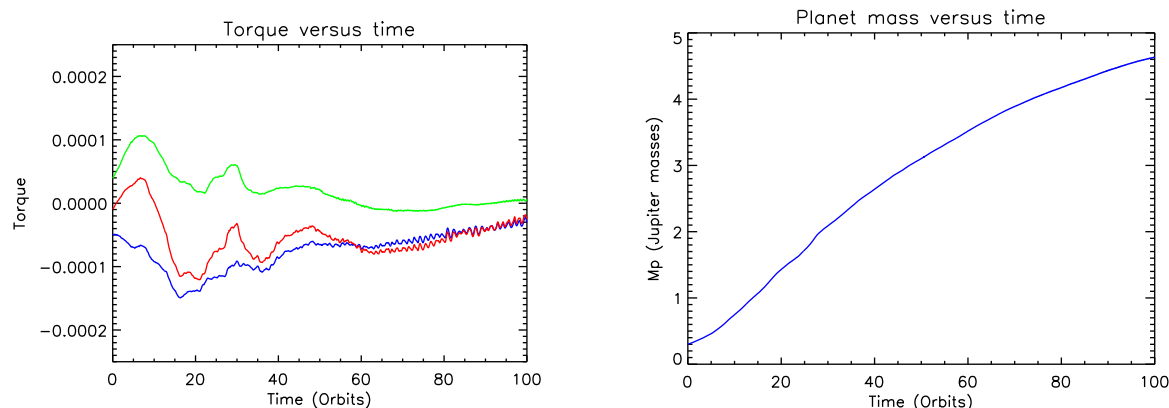


Fig. 17 The left panel shows the torque experienced by the giant as a function of time. The right panel shows the evolution of the giant planet mass as it accretes gas from the disc.

possible, allowing the influence of magnetohydrodynamic turbulence on planet formation and migration to be studied.

Key questions for the future relate to how these various physical effects combine to change our current understanding of planetary migration. For example, the long-term action of corotation torques requires viscous diffusion to operate in the disc in order to prevent saturation. An important question is how these corotation torques operate in discs where the effective viscous stresses are provided by magnetohydrodynamic turbulence? Can the corotation torques remain unsaturated within a dead zone? These and other important questions are the subject of on-going research. The increasing power of available computing facilities will continue to facilitate the development of increasingly realistic disc models, which will in turn lead to an increase in our understanding of planetary formation and migration.

References

1. Beckwith, S.V.W., Sargent, A.I.: Circumstellar disks and the search for neighbouring planetary systems. *Nature* **383**, 139–144 (1996). DOI 10.1038/383139a0
2. Pollack, J.B., Hubickyj, O., Bodenheimer, P., Lissauer, J.J., Podolak, M., Greenzweig, Y.: Formation of the Giant Planets by Concurrent Accretion of Solids and Gas. *Icarus* **124**, 62–85 (1996). DOI 10.1006/icar.1996.0190
3. Mayor, M., Queloz, D.: A Jupiter-Mass Companion to a Solar-Type Star. *Nature* **378**, 355–359 (1995). DOI 10.1038/378355a0
4. Goldreich, P., Tremaine, S.: The excitation of density waves at the Lindblad and corotation resonances by an external potential. *Astrophysical Journal* **233**, 857–871 (1979). DOI 10.1086/157448
5. Goldreich, P., Tremaine, S.: Disk-satellite interactions. *Ap.J.* **241**, 425–441 (1980). DOI 10.1086/158356
6. Lin, D.N.C., Papaloizou, J.: Tidal torques on accretion discs in binary systems with extreme mass ratios. *MNRAS* **186**, 799–812 (1979)
7. Lin, D.N.C., Papaloizou, J.: On the tidal interaction between protoplanets and the protoplanetary disk. III - Orbital migration of protoplanets. *Ap.J.* **309**, 846–857 (1986). DOI 10.1086/164653
8. Masset, F.S., Papaloizou, J.C.B.: Runaway Migration and the Formation of Hot Jupiters. *Astrophysical Journal* **588**, 494–508 (2003). DOI 10.1086/373892
9. Tanaka, H., Takeuchi, T., Ward, W.R.: Three-Dimensional Interaction between a Planet and an Isothermal Gaseous Disk. I. Corotation and Lindblad Torques and Planet Migration. *Astrophysical Journal* **565**, 1257–1274 (2002). DOI 10.1086/324713
10. Nelson, R.P., Papaloizou, J.C.B.: The interaction of giant planets with a disc with MHD turbulence - IV. Migration rates of embedded protoplanets. *Monthly Notices of the Royal Astronomical Society* **350**, 849–864 (2004). DOI 10.1111/j.1365-2966.2004.07406.x
11. Ward, W.R.: Protoplanet Migration by Nebula Tides. *Icarus* **126**, 261–281 (1997). DOI 10.1006/icar.1996.5647
12. Goodman, J., Rafikov, R.R.: Planetary Torques as the Viscosity of Protoplanetary Disks. *Astrophysical Journal* **552**, 793–802 (2001). DOI 10.1086/320572
13. Ida, S., Lin, D.N.C.: Toward a Deterministic Model of Planetary Formation. IV. Effects of Type I Migration. *Astrophysical Journal* **673**, 487–501 (2008). DOI 10.1086/523754
14. Bate, M.R., Lubow, S.H., Ogilvie, G.I., Miller, K.A.: Three-dimensional calculations of high- and low-mass planets embedded in protoplanetary discs. *Monthly Notices of the Royal Astronomical Society* **341**, 213–229 (2003). DOI 10.1046/j.1365-8711.2003.06406.x
15. Terquem, C.E.J.M.L.J.: Stopping inward planetary migration by a toroidal magnetic field. *Monthly Notices of the Royal Astronomical Society* **341**, 1157–1173 (2003). DOI 10.1046/j.1365-8711.2003.06455.x
16. Pierens, A., Huré, J.M.: How does disk gravity really influence type-I migration? *Astronomy and Astrophysics* **433**, L37–L40 (2005). DOI 10.1051/0004-6361:200500099
17. Baruteau, C., Masset, F.: Type I Planetary Migration in a Self-Gravitating Disk. *Astrophysical Journal* **678**, 483–497 (2008). DOI 10.1086/529487
18. Paardekooper, S.J., Mellema, G.: Halting type I planet migration in non-isothermal disks. *Astronomy and Astrophysics* **459**, L17–L20 (2006). DOI 10.1051/0004-6361:20066304
19. Baruteau, C., Masset, F.: On the Corotation Torque in a Radiatively Inefficient Disk. *Astrophysical Journal* **672**, 1054–1067 (2008). DOI 10.1086/523667
20. Paardekooper, S.J., Papaloizou, J.C.B.: On disc protoplanet interactions in a non-barotropic disc with thermal diffusion. *Astronomy and Astrophysics* **485**, 877–895 (2008). DOI 10.1051/0004-6361:20078702
21. Ward, W.R.: Horseshoe Orbit Drag. In: *Lunar and Planetary Insti-*

- tute Conference Abstracts, *Lunar and Planetary Institute Conference Abstracts*, vol. 22, pp. 1463–1464 (1991)
22. Paardekooper, S.J., Papaloizou, J.C.B.: On the width and shape of the corotation region for low-mass planets. *MNRAS***394**, 2297–2309 (2009). DOI 10.1111/j.1365-2966.2009.14512.x
 23. Paardekooper, S.J., Papaloizou, J.C.B.: On corotation torques, horseshoe drag and the possibility of sustained stalled or outward protoplanetary migration. *MNRAS***394**, 2283–2296 (2009). DOI 10.1111/j.1365-2966.2009.14511.x
 24. Paardekooper, S.J., Mellema, G.: Growing and moving low-mass planets in non-isothermal disks. *Astronomy and Astrophysics* **478**, 245–266 (2008). DOI 10.1051/0004-6361:20078592
 25. Ogilvie, G.I., Lubow, S.H.: Saturation of the Corotation Resonance in a Gaseous Disk. *Astrophysical Journal* **587**, 398–406 (2003). DOI 10.1086/368178
 26. Masset, F.S.: On the Co-orbital Corotation Torque in a Viscous Disk and Its Impact on Planetary Migration. *Ap.J.***558**, 453–462 (2001). DOI 10.1086/322446
 27. Kley, W., Crida, A.: Migration of protoplanets in radiative discs. *A & A***487**, L9–L12 (2008). DOI 10.1051/0004-6361:200810033
 28. Pepliński, A., Artymowicz, P., Mellema, G.: Numerical simulations of type III planetary migration - II. Inward migration of massive planets. *Monthly Notices of the Royal Astronomical Society* **386**, 179–198 (2008). DOI 10.1111/j.1365-2966.2008.13046.x
 29. Papaloizou, J.C.B., Nelson, R.P., Kley, W., Masset, F.S., Artymowicz, P.: Disk-Planet Interactions During Planet Formation. In: B. Reipurth, D. Jewitt, K. Keil (eds.) *Protostars and Planets V*, pp. 655–668 (2007)
 30. Pepliński, A.: Numerical simulations of type III planetary migration. Ph.D. thesis, Department of Astronomy, Stockholm University, Stockholm (2008)
 31. Pepliński, A., Artymowicz, P., Mellema, G.: Numerical simulations of type III planetary migration - III. Outward migration of massive planets. *Monthly Notices of the Royal Astronomical Society* **387**, 1063–1079 (2008). DOI 10.1111/j.1365-2966.2008.13339.x
 32. D’Angelo, G., Bate, M.R., Lubow, S.H.: The dependence of protoplanet migration rates on co-orbital torques. *Monthly Notices of the Royal Astronomical Society* **358**, 316–332 (2005). DOI 10.1111/j.1365-2966.2005.08866.x
 33. Pepliński, A., Artymowicz, P., Mellema, G.: Numerical simulations of type III planetary migration - I. Disc model and convergence tests. *Monthly Notices of the Royal Astronomical Society* **386**, 164–178 (2008). DOI 10.1111/j.1365-2966.2008.13045.x
 34. Crida, A., Morbidelli, A., Masset, F.: On the width and shape of gaps in protoplanetary disks. *Icarus* **181**, 587–604 (2006). DOI 10.1016/j.icarus.2005.10.007
 35. Lin, D.N.C., Papaloizou, J.C.B.: On the tidal interaction between protostellar disks and companions. In: E.H. Levy, J.I. Lunine (eds.) *Protostars and Planets III*, pp. 749–835 (1993)
 36. Bryden, G., Chen, X., Lin, D.N.C., Nelson, R.P., Papaloizou, J.C.B.: Tidally Induced Gap Formation in Protostellar Disks: Gap Clearing and Suppression of Protoplanetary Growth. *Ap.J.***514**, 344–367 (1999). DOI 10.1086/306917
 37. Nelson, R.P., Papaloizou, J.C.B., Masset, F., Kley, W.: The migration and growth of protoplanets in protostellar discs. *MNRAS***318**, 18–36 (2000). DOI 10.1046/j.1365-8711.2000.t01-1-03605.x
 38. Kley, W.: Mass flow and accretion through gaps in accretion discs. *MNRAS***303**, 696–710 (1999). DOI 10.1046/j.1365-8711.1999.02198.x
 39. D’Angelo, G., Henning, T., Kley, W.: Nested-grid calculations of disk-planet interaction. *A & A***385**, 647–670 (2002). DOI 10.1051/0004-6361:20020173
 40. Kley, W., D’Angelo, G., Henning, T.: Three-dimensional Simulations of a Planet Embedded in a Protoplanetary Disk. *Ap.J.***547**, 457–464 (2001). DOI 10.1086/318345
 41. D’Angelo, G., Kley, W., Henning, T.: Orbital Migration and Mass Accretion of Protoplanets in Three-dimensional Global Computations with Nested Grids. *Ap.J.***586**, 540–561 (2003). DOI 10.1086/367555
 42. Ivanov, P.B., Papaloizou, J.C.B., Polnarev, A.G.: The evolution of a supermassive binary caused by an accretion disc. *MNRAS***307**, 79–90 (1999). DOI 10.1046/j.1365-8711.1999.02623.x
 43. Snellgrove, M.D., Papaloizou, J.C.B., Nelson, R.P.: On disc driven inward migration of resonantly coupled planets with application to the system around GJ876. *A & A***374**, 1092–1099 (2001). DOI 10.1051/0004-6361:20010779
 44. Crida, A., Sándor, Z., Kley, W.: Influence of an inner disc on the orbital evolution of massive planets migrating in resonance. *A & A***483**, 325–337 (2008). DOI 10.1051/0004-6361:20079291
 45. Zhang, H., Yuan, C., Lin, D.N.C., Yen, D.C.C.: On the Orbital Evolution of a Jovian Planet Embedded in a Self-Gravitating Disk. *Astrophysical Journal* **676**, 639–650 (2008). DOI 10.1086/528707
 46. Balbus, S.A., Hawley, J.F.: A powerful local shear instability in weakly magnetized disks. I - Linear analysis. II - Nonlinear evolution. *Ap.J.***376**, 214–233 (1991). DOI 10.1086/170270
 47. Balbus, S.A., Hawley, J.F.: Instability, turbulence, and enhanced transport in accretion disks. *Reviews of Modern Physics* **70**, 1–53 (1998). DOI 10.1103/RevModPhys.70.1
 48. Papaloizou, J.C.B., Nelson, R.P.: The interaction of a giant planet with a disc with MHD turbulence - I. The initial turbulent disc models. *MNRAS***339**, 983–992 (2003). DOI 10.1046/j.1365-8711.2003.06246.x
 49. Miller, K.A., Stone, J.M.: The Formation and Structure of a Strongly Magnetized Corona above a Weakly Magnetized Accretion Disk. *Ap.J.***534**, 398–419 (2000). DOI 10.1086/308736
 50. Fromang, S., Nelson, R.P.: Global MHD simulations of stratified and turbulent protoplanetary discs. I. Model properties. *A & A***457**, 343–358 (2006). DOI 10.1051/0004-6361:20065643
 51. Fromang, S., Papaloizou, J., Lesur, G., Heinemann, T.: MHD simulations of the magnetorotational instability in a shearing box with zero net flux. II. The effect of transport coefficients. *A & A***476**, 1123–1132 (2007). DOI 10.1051/0004-6361:20077943
 52. Lesur, G., Longaretti, P.Y.: Impact of dimensionless numbers on the efficiency of magnetorotational instability induced turbulent transport. *MNRAS***378**, 1471–1480 (2007). DOI 10.1111/j.1365-2966.2007.11888.x
 53. Gammie, C.F.: Layered Accretion in T Tauri Disks. *Ap.J.***457**, 355–+ (1996). DOI 10.1086/176735
 54. Fromang, S., Terquem, C., Balbus, S.A.: The ionization fraction in α models of protoplanetary discs. *MNRAS***329**, 18–28 (2002). DOI 10.1046/j.1365-8711.2002.04940.x
 55. Ilgner, M., Nelson, R.P.: On the ionisation fraction in protoplanetary disks. I. Comparing different reaction networks. *A & A***445**, 205–222 (2006). DOI 10.1051/0004-6361:20053678
 56. Ilgner, M., Nelson, R.P.: Turbulent transport and its effect on the dead zone in protoplanetary discs. *A & A***483**, 815–830 (2008). DOI 10.1051/0004-6361:20079307
 57. Papaloizou, J.C.B., Nelson, R.P., Snellgrove, M.D.: The interaction of giant planets with a disc with MHD turbulence - III. Flow morphology and conditions for gap formation in local and global simulations. *MNRAS***350**, 829–848 (2004). DOI 10.1111/j.1365-2966.2004.07566.x
 58. Nelson, R.P.: On the orbital evolution of low mass protoplanets in turbulent, magnetised disks. *A & A***443**, 1067–1085 (2005). DOI 10.1051/0004-6361:20042605
 59. Laughlin, G., Steinacker, A., Adams, F.C.: Type I Planetary Migration with MHD Turbulence. *Ap.J.***608**, 489–496 (2004). DOI 10.1086/386316
 60. Masset, F.S., Morbidelli, A., Crida, A., Ferreira, J.: Disk Surface Density Transitions as Protoplanet Traps. *Ap.J.***642**, 478–487 (2006). DOI 10.1086/500967

-
61. Nelson, R.P., Papaloizou, J.C.B.: The interaction of a giant planet with a disc with MHD turbulence - II. The interaction of the planet with the disc. *MNRAS***339**, 993–1005 (2003). DOI 10.1046/j.1365-8711.2003.06247.x
 62. Winters, W.F., Balbus, S.A., Hawley, J.F.: Gap Formation by Planets in Turbulent Protostellar Disks. *Ap.J.***589**, 543–555 (2003). DOI 10.1086/374409

